MRI Compatibility of a High-Resolution Small Animal PET Insert Operating Inside a 7T MRI

Jonathan D. Thiessen[1,2], Ehsan Shams[3,4], Greg Stortz[5], Graham Schellenberg[4], Daryl Bishop[6], Muhammad Salman Khan[7], Piotr Kozlowski[8], Fabrice Retière[6], Vesna Sossi[5], Christopher J. Thompson[9], and Andrew L. Goertzen[4,10]

[1]Imaging Program, Lawson Health Research Institute, London, Ontario, Canada, [2]Medical Biophysics, Western University, London, Ontario, Canada, [3]Graduate Program in Biomedical Engineering, University of Manitoba, Winnipeg, Manitoba, Canada, [4]Physics & Astronomy, University of Manitoba, Winnipeg, Manitoba, Canada, [5]Physics & Astronomy, University of British Columbia, Vancouver, British Columbia, Canada, [6]Detector Development Group, TRIUMF, Vancouver, British Columbia, Canada, [7]Electrical & Computer Engineering, University of Manitoba, Winnipeg, Manitoba, Canada, [8]Radiology, University of British Columbia, Vancouver, British Columbia, Canada, [9]McConnell Brain Imaging Centre, Montreal Neurological Institute, Montréal, Québec, Canada, [10]Radiology, University of Manitoba, Winnipeg, Manitoba, Canada

Target Audience: Engineers and scientists interested in high-resolution, simultaneous PET/MRI of small animals.

Purpose: We are building an MRI compatible, small animal positron emission tomography (PET) insert that features a ring of 16 detector modules. The PET insert is designed to achieve 1 mm spatial resolution in the center of its field-of-view (FOV)[1,2] and fit within the 114 mm inner diameter (ID) of a BGA-12S gradient system installed in a Bruker 7T MRI. PET detector and MRI performance was evaluated with the PET insert installed and operational.

Methods: ***PET Detector Modules and Gantry:*** Each detector module has two MR-compatible silicon photomultipler (SiPM) arrays (SensL ArraySB-4), a 32:4 multiplexing resistor network, two differential amplifiers (Analog Devices ADA4932-2), temperature monitoring (Microchip TC1047), and a Type C High-Definition Multimedia Interface (Mini-HDMI) receptacle for signal and power transmission. A 28.3x13 mm, dual-layer scintillator crystal array converts 511 keV photons into visible light and is optically coupled to the SiPMs. Each scintillator array has a 22x10/6-mm thick bottom array and a 21x9/4-mm thick top array of Cerium-doped Lutetium Yttrium Orthosilicate (LYSO) crystals separated by specular reflector (409 crystals total). Detector boards are mounted onto copper-clad PCB with non-magnetic brass and nylon components and then fastened to a PET gantry consisting of CNC-milled ABS supports attached to a 60 mm ID carbon fiber cylinder (**Fig. A**). RF shielding consists of 35 µm thick copper foil, segmented by 1-mm gaps between blocks. The RF shielding for each detector module is grounded via the HDMI receptacle. Electrical continuity is maintained via the carbon fiber cylinder, which is slightly conductive with ~10Ω resistance between copper segments. A 113 mm outer diameter carbon fiber cylinder makes the completed PET insert light tight (**Fig. B**). SiPM gain and LYSO light output are both temperature dependent, thus, temperature is actively monitored and detector gain controlled with a custom detector control system[3]. During the initial tests, all 16 detectors were powered, but singles data were acquired from just two detectors at a time with a ^{22}Na point source using a series of NIM electronics and a PC-based ADC card. ***MRI:*** A 50mL, H_2O phantom containing 1 g/l Cu_2SO_4•$5H_2O$ and 3.6 g/l NaCl was imaged using a quadrature volume RF coil with a 35 mm ID (Bruker) in a 7 T Bruker Avance III MRI system. A series of 3D FLASH images with different echo times and flip angles were acquired to generate B_0 and B_1 field maps[4] with a 3.5x3.5x7 cm FOV encompassing the volume of the phantom visible in the RF coil. To evaluate MR image quality, 11 slices were placed along the extent of the phantom with a 1 mm slice thickness and 3.5x3.5 cm in-plane FOV. Spin echo (SE), RARE, FLASH, and single-shot echo planar images (EPI) were acquired. ***PET/MRI:*** MRI sequences were repeated with 3 different setups: MRI only (**M**), MRI with the PET insert present, but not operating (**MP**), and MRI with the PET insert operating (**MPO**). PET detector data were acquired both outside and inside the MRI with a ^{22}Na point source centered in the phantom. MRI acquisitions were repeated without a source present to reduce distortions in the MR images. Crystal flood histograms were created using one of the PET detectors with energy resolution calculated as the full width at half maximum (FWHM) of the 511 keV photopeak normalized to the photopeak voltage for each of the 409 crystals identified in the flood histogram.

Results and Discussion: The operating PET insert (MPO) had no effect on image homogeneity and only a small effect on EPI SNR (-15%), where rapidly changing gradient fields could induce eddy currents on the conductive components of the PET insert (**Fig. C**). B_1 field maps represent the accuracy of a α=90° RF pulse and show no significant difference with MPO (**Fig. D**). B_0 field maps represent the deviation from the Larmor frequency ($\Delta\omega$). Mean $\Delta\omega/\omega$ was slightly large with MPO (0.27 ppm) when compared to MRI only (0.16 ppm) (**Fig. E**). There was no observable difference in PET detector flood quality (**Fig. F**) and mean energy resolution per crystal was 13±2% both outside the MRI and inside during different pulse sequences (**Fig. G**). After 2 hours of operation, temperature stabilized at ~31 and 33 °C for detector modules at the bottom and top of the PET insert, respectively. Temperature-dependent detector gain will be stabilized using the detector control system to account for this temperature gradient[3].

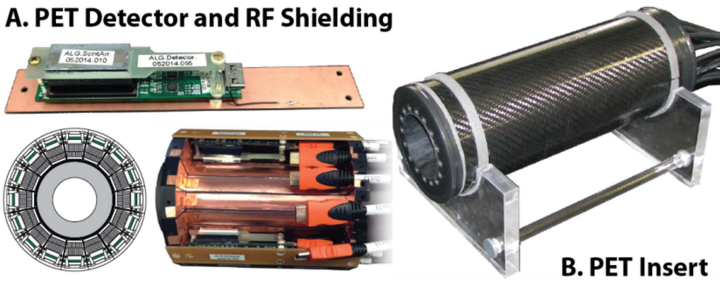

C. MRI

	SNR			Image Homogeneity (%)		
	M	MP	MPO	M	MP	MPO
SE	148 ± 10	157 ± 6	154 ± 3	94.8 ± 0.3	94.5 ± 0.3	94.5 ± 0.3
RARE	250 ± 13	243 ± 13	250 ± 13	91.3 ± 0.9	90.0 ± 1.7	91.6 ± 0.6
FLASH	74 ± 2	75 ± 2	74 ± 2	88.3 ± 0.9	88.6 ± 0.7	88.2 ± 0.6
EPI	188 ± 4	159 ± 12	164 ± 9	40.6 ± 0.3	40.6 ± 0.1	40.6 ± 0.2

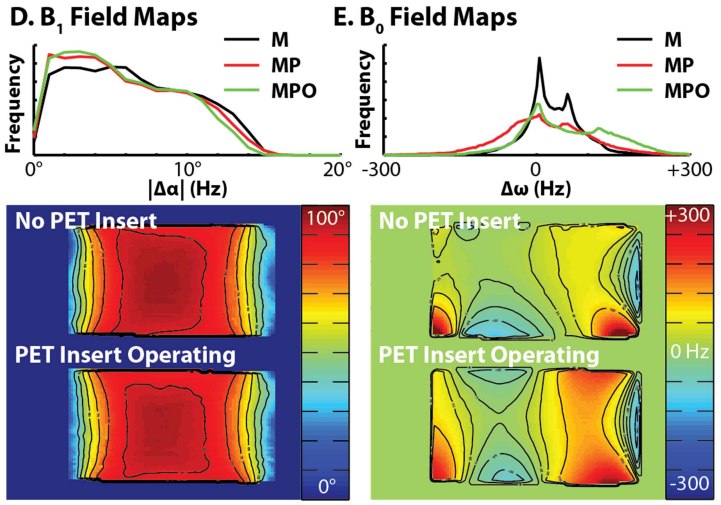

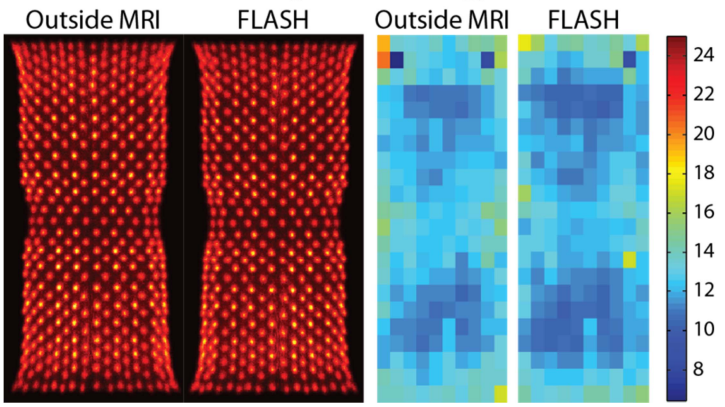

Conclusion and Future Work: Good PET detector and MRI performance was demonstrated with the PET insert operating inside a Bruker 7T MRI. A data acquisition system capable of acquiring energy data from all 16 detector modules is currently being developed on the OpenPET firmware platform[5], with the first PET/MR images anticipated in early 2015.

References: 1. Zhang, PMB **58** (2013), 2. Stortz, IEEE TNS **60** (2013), 3. Shams IEEE MIC (2014), 4. Dowell, MRM **58** (2007), 5. Moses, IEEE TNS (2009)